

Novel approach to pion and eta production in proton-proton collisions

V. Bernard[†], N. Kaiser[◦], Ulf-G. Meißner[†]

[†]Université Louis Pasteur, Laboratoire de Physique Théorique
3-5, rue de l’Université, F-67084 Strasbourg, France
email: *bernard@lpt1.u-strasbg.fr*

[◦]Technische Universität München, Physik Department T39
James-Franck-Straße, D-85747 Garching, Germany
email: *nkaiser@physik.tu-muenchen.de*

[†]Forschungszentrum Jülich, Institut für Kernphysik (Theorie)
D-52425 Jülich, Germany
email: *Ulf-G.Meissner@fz-juelich.de*

Abstract

We evaluate the threshold matrix-element for the reaction $pp \rightarrow pp\pi^0$ in a fully relativistic Feynman diagrammatic approach. We employ a simple effective range approximation to take care of the S-wave pp final-state interaction. The experimental value for the threshold amplitude $\mathcal{A} = (2.7 - i 0.3) \text{ fm}^4$ can be reproduced by contributions from tree level chiral (long-range) pion exchange and short-range effects related to heavy meson exchanges, with these two very different contributions of roughly the same size. Pion loop effects appear to be small. We stress that the commonly used heavy baryon formalism is not applicable in the NN-system above the pion production threshold due to the large external momentum, $|\vec{p}| \simeq \sqrt{mM_\pi}$, with m and M_π the nucleon and the pion mass, respectively. We furthermore investigate the reaction $pp \rightarrow pn\pi^+$ near threshold within the same approach. We extract from the data the triplet threshold amplitude, $\mathcal{B} = (3.9 - i 2.1) \text{ fm}^4$, which comes out too small by a factor of two from tree level diagrams. A reason why this approach works well for $pp \rightarrow pp\pi^0$ and less well for $pp \rightarrow pn\pi^+$ is the relative strength of initial-state interactions. In addition, we investigate the process $pp \rightarrow pp\eta$ near threshold. We use a simple factorization ansatz for the $pp\eta$ final-state interaction and extract from the data the modulus of the threshold amplitude, $|\mathcal{C}| = 1.32 \text{ fm}^4$. With $g_{\eta N} = 5.3$, this value can be reproduced by tree level meson exchange diagrams and η -rescattering, whose strength is fixed by the ηN scattering length. We also comment on the recent near threshold data for η' -production.

1 Introduction and summary

With the advent of proton cooler synchrotrons at Bloomington, Jülich and Uppsala, high precision data for the processes $pp \rightarrow pp\pi^0$, $pp \rightarrow d\pi^+$, $pp \rightarrow pn\pi^+$ and $pp \rightarrow pp\eta$ in the threshold region [1, 2, 3, 4, 5] have become available. The first data on neutral pion production were a big surprise because the experimental cross sections turned out to be a factor of five larger than the theoretical predictions based on direct pion production and neutral pion rescattering fixed from on-shell πN data. Nevertheless, the energy-dependence of the total cross section σ_{tot} from threshold to excess energies of about 50 MeV is completely given by the strong S-wave pp final-state interaction, see e.g. ref.[6]. Subsequently, it was argued that heavy-meson exchanges might be able to remove this discrepancy [7, 8]. On the other hand it was shown [9, 10] that the (model-dependent) off-shell behavior of the full πN T-matrix also can enhance the cross section considerably. Another avenue to eventually understand the near threshold cross section is offered by calculations within the framework of tree-level heavy baryon chiral perturbation theory (HBChPT) including dimension two operators [11, 12, 13, 14]. In these papers, HBChPT has been used to constrain the long-range π^0 -exchange contributions. However, it was found that the calculations for $pp \rightarrow pp\pi^0$ performed so far lead to a marked difference in the role of the so-called π^0 rescattering contribution, which interferes constructively with the direct production in the Jülich model and destructively in the HBChPT framework, respectively. In a recent paper, it was argued that the treatment underlying the isoscalar pion-nucleon scattering amplitude and the related transition operator for the process $NN \rightarrow NN\pi$ (where N denotes the nucleon) in the HBChPT framework is not yet sufficiently accurate and thus the resulting rescattering contribution should be considered as an artifact of this approximation [15]. It was also stressed that the process $pp \rightarrow d\pi^+$ is more sensitive to the long-range (chiral) pion exchange. One-loop graphs have been considered in [16].

However, one important feature of this reaction should be kept in mind, namely the large momentum mismatch between the initial and the final nucleon-nucleon state: the initial center-of-mass momentum is given by $|\vec{p}|^2 = m M_\pi + M_\pi^2/4$, with M_π (m) the neutral pion (proton) mass, whereas close to threshold the final one is compatible with zero. This large difference leads to momentum transfers equal to $|\vec{p}|$ and higher. In particular, both the squared invariant momentum transfer and the kinetic energy of the incoming protons are $-m M_\pi$ and $M_\pi/2$, respectively, and therefore the chiral counting in the original sense does not apply, see e.g. [12]. We will actually demonstrate here that non-relativistic approximations (i.e. the heavy baryon formalism or HBChPT) are not applicable in the two-nucleon system above the pion production threshold. The simple reason for that is the extreme kinematics with the external momentum $|\vec{p}| \simeq \sqrt{m M_\pi}$ diverging in the heavy nucleon limit $m \rightarrow \infty$ (while this argument could be considered formal, it nicely pinpoints the problems of the heavy baryon approach.). The HBChPT framework (which is very successful for low-energy single nucleon processes) loses its systematic order-by-order low-energy expansion when external momenta grow with the nucleon mass ($|\vec{p}| \sim \sqrt{m}$). In order to avoid such problems (which are simply related to kinematics) it seems mandatory to perform fully relativistic calculations. In particular, we find that one of the low-energy constants c_2 entering the chiral π^0 -rescattering is enhanced in the relativistic calculation by a factor of two as compared to the non-relativistic HBChPT approach. In this spirit we perform here a fully relativistic calculation of various tree and one-loop diagrams contributing to $pp \rightarrow pp\pi^0$ and $pp \rightarrow pn\pi^+$ at threshold. Our

approach can also be extended in a straightforward manner to η and η' production in pp –collisions. We thus discuss here also the reaction $pp \rightarrow pp\eta$ up to excess energies of about 100 MeV using a simple factorized form to account for the final–state interactions in the $pp\eta$ three–body system.

The pertinent results of this investigation can be summarized as follows:

- (i) Assuming that the pp final–state interaction is an on–shell NN–process and using a simple effective range parametrization for the pp 1S_0 phase shift, we can accurately fit the 40 data points of the total cross section from threshold up to $T_{\text{lab}} = 326$ MeV with a constant (threshold) amplitude equal to $\mathcal{A} = (2.7 - i 0.3)$ fm 4 .
- (ii) This number can be well understood in terms of chiral π^0 exchange (including chiral π^0 rescattering) and heavy meson (ω , ρ^0 , η) exchanges based on a relativistic Feynman diagram calculation.
- (iii) We have evaluated some classes of one-loop graphs and find that they lead to small corrections of the order of a few percent. Therefore chiral loops do not seem to play any significant role in the processes $NN \rightarrow NN\pi$, which are dominated by one–pion exchange and short–range physics (with the notable exception of $pp \rightarrow d\pi^+$, where d denotes the deuteron).
- (iv) Both the long range π^0 exchange and the short range vector meson exchange lead to contributions to the threshold amplitude \mathcal{A} which do not vanish in the chiral limit $M_\pi \rightarrow 0$. There is no chiral suppression of the reaction $pp \rightarrow pp\pi^0$ compared to other $NN\pi$ channels. In all cases the respective threshold amplitudes are non-zero (and finite) in the chiral limit. This is in contrast to the widespread belief that $pp \rightarrow pp\pi^0$ is suppressed for reasons of chiral symmetry.
- (v) Within the same approach, we have investigated the threshold behavior of the process $pp \rightarrow pn\pi^+$. It is given in terms of \mathcal{A} and the triplet threshold amplitude \mathcal{B} . Only about half of the magnitude of \mathcal{B} is reproduced by chiral one–pion exchange and short–range vector meson physics. The empirical value of \mathcal{B} has a sizeable imaginary part, which naturally can not be explained by tree graphs only. This channel deserves further study.
- (vi) The good description of the channel $pp \rightarrow pp\pi^0$ and the less good description of the channel $pp \rightarrow pn\pi^+$ within our diagrammatic approach can be understood from the relative strengths of the initial–state interaction. It is weak in the 3P_0 entrance channel and strong in the 3P_1 entrance channel.
- (vii) Finally, we have investigated the process $pp \rightarrow pp\eta$ near threshold. We treat the final state–interaction in the pp and ηp subsystems using a factorization ansatz and effective range approximations. The empirical value of the modulus of the threshold amplitude, $|\mathcal{C}| = 1.32$ fm 4 , is reproduced with $g_{\eta N} = 5.3$ by tree level meson exchange graphs and η –rescattering. The strength of the latter is fixed from the (real part of the) ηN scattering length.

2 Threshold kinematics and final-state interaction

2.1 Kinematics

We consider the reaction $p_1(\vec{p}) + p_2(-\vec{p}) \rightarrow p + p + \pi^0$ in the center-of-mass (cm) frame at threshold. The invariant T-matrix can be expressed in terms of one complex-valued (constant) amplitude, which we denote by \mathcal{A} , as (see fig. 1)

$$T_{\text{th}}^{\text{cm}}(pp \rightarrow pp\pi^0) = \mathcal{A} (i\vec{\sigma}_1 - i\vec{\sigma}_2 + \vec{\sigma}_1 \times \vec{\sigma}_2) \cdot \vec{p} . \quad (1)$$

The $\vec{\sigma}_{1,2}$ are the spin-matrices of the two protons. The value of the proton cm momentum to produce a neutral pion at rest is given by

$$|\vec{p}| = \sqrt{M_\pi(m + M_\pi/4)} = 362.2 \text{ MeV} , \quad (2)$$

with $m = 938.27$ MeV the proton and $M_\pi = 134.97$ MeV the neutral pion mass, respectively. Obviously, $|\vec{p}|$ vanishes in the chiral limit of zero pion mass. Therefore the soft-pion theorem which requires a vanishing threshold T-matrix in the chiral limit $M_\pi = 0$ is trivially fulfilled (as long as \mathcal{A} does not become singular) [17]. We remark that similar features occur for the reaction $\pi N \rightarrow \pi\pi N$ (see ref.[18]). All dynamical information is encoded in the threshold amplitude \mathcal{A} of dimension [length⁴]. In the threshold region, the wave function of the final di-proton system as well as that of the neutral pion are dominated by angular momentum zero states, thus we are dealing with a ${}^3P_0 \rightarrow {}^1S_0 s$ transition. Consequently, one deduces from unitarity

$$\mathcal{A} = |\mathcal{A}| e^{i\delta({}^3P_0)} , \quad (3)$$

with the 3P_0 pp phase shift to be taken at the threshold energy in the lab frame, $T_{\text{th}}^{\text{lab}} = 279.65$ MeV, where $\delta({}^3P_0) = -6.3^\circ$. Thus the imaginary part $\text{Im } \mathcal{A}$ is about $-1/9$ of the real part $\text{Re } \mathcal{A}$ and contributes negligibly to the total cross section near threshold proportional to $|\mathcal{A}|^2$. The threshold T-matrix is a pseudoscalar, it is symmetric under the exchange of the two ingoing protons $\vec{\sigma}_1 \leftrightarrow \vec{\sigma}_2$, $\vec{p} \rightarrow -\vec{p}$. Furthermore Eq.(1) incorporates the Pauli exclusion principle for the (indistinguishable) outgoing protons, since left multiplication with the spin exchange operator $(1 + \vec{\sigma}_1 \cdot \vec{\sigma}_2)/2$ leads to a minus sign by the identity: $\frac{1}{2}(1 + \vec{\sigma}_1 \cdot \vec{\sigma}_2)(i\vec{\sigma}_1 - i\vec{\sigma}_2 + \vec{\sigma}_1 \times \vec{\sigma}_2) = -(\vec{\sigma}_1 \times \vec{\sigma}_2 + i\vec{\sigma}_1 - i\vec{\sigma}_2)$. Diagrams with crossed proton lines are therefore automatically included. Approximating the near threshold T-matrix by the T-matrix exactly at threshold one gets for the unpolarized total cross section

$$\sigma_{\text{tot}}(T_{\text{lab}}) = \frac{m^4 \mu \sqrt{4 + \mu}}{16\pi^2 (2 + \mu)^{9/2}} |\mathcal{A}|^2 (T_{\text{lab}} - T_{\text{th}}^{\text{lab}})^2 , \quad (4)$$

with $\mu = M_\pi/m$. Note that the flux and three-body phase space factors have been approximated in Eq.(4) by an analytical expression which is accurate within a few percent in the threshold region. Such a form has already been proven to be quite accurate in chiral perturbation theory studies of the reactions $\gamma p \rightarrow \pi^0 \pi^0 p$ [19] and $\pi N \rightarrow \pi\pi N$ [20], where γ denotes a real photon. In the case of $pp \rightarrow pp\pi^0$, however, such an approximation is not sufficient near threshold. This can be seen e.g. by taking the near threshold data of refs. [1, 2] and dividing them by the three-body phase space factor $\sim (T_{\text{lab}} - T_{\text{th}}^{\text{lab}})^2$, i.e. $\sigma_{\text{tot}}(T_{\text{lab}}) = C \cdot (T_{\text{lab}} - T_{\text{th}}^{\text{lab}})^2$. The resulting values for C are not constant in energy. This, of course, has to do with the strong pp final-state interaction in the 1S_0 partial wave. So before we can extract a value for $|\mathcal{A}|$, we have to correct for the final-state interaction.

2.2 Treatment of the final-state interaction

The final-state interaction in the 1S_0 di-proton state modifies the simple phase-space formula Eq.(4). We follow here a procedure derived by Watson [21] where one essentially assumes that final-state interaction is taking place only when the nucleons are on their mass-shell. In this approach, the unpolarized total cross section for $pp \rightarrow pp\pi^0$ including final-state interaction takes the form

$$\begin{aligned} \sigma_{\text{tot}}(T_{\text{lab}}) &= |\mathcal{A}|^2 \left(\frac{m}{4\pi}\right)^3 \frac{2\sqrt{T_{\text{lab}}}}{(2m + T_{\text{lab}})^{3/2}} \\ &\times \int_{2m}^{W_{\text{max}}} dW \sqrt{(W^2 - 4m^2) \lambda(W^2, M_\pi^2, 4m^2 + 2mT_{\text{lab}})} F_p(W) . \end{aligned} \quad (5)$$

Here, $F_p(W)$ is the correction factor due the final-state interaction. We evaluate it in the effective range approximation. This is of course a very strong assumption but it allows to explain the energy dependence of the experimental total cross sections very accurately in terms of a single constant amplitude \mathcal{A} . Separating off the final-state interaction in that way, we can then pursue a diagrammatic approach to the (on-shell) production amplitude \mathcal{A} . This will allow us to investigate in a simple fashion the role of one-pion exchange and chiral loop effects together with shorter range exchanges due to heavier mesons. For a more complete dynamical description including off-shell final-state interactions and so on, a microscopic model treating also (unobservable) half-off shell effects is needed. After these remarks, we return to the effective range approximation, in which the function $F_p(W)$ takes the form

$$F_p(W) = \frac{4 \sin^2 \delta_0(W)}{a_p^2 (W^2 - 4m^2)} = \left\{ 1 + \frac{a_p}{4} (a_p + r_p) (W^2 - 4m^2) + \frac{a_p^2 r_p^2}{64} (W^2 - 4m^2)^2 \right\}^{-1} \quad (6)$$

with W the final-state di-proton invariant mass and $\lambda(x, y, z) = x^2 + y^2 + z^2 - 2yz - 2xz - 2xy$ the Källen function. $W_{\text{max}} = \sqrt{4m^2 + 2mT_{\text{lab}}} - M_\pi$ is the kinematical endpoint of the di-proton invariant mass spectrum. Furthermore, $a_p = (7.8098 \pm 0.0023)$ fm and $r_p = (2.767 \pm 0.010)$ fm, taken from ref.[22], are the scattering length and effective range parameter for elastic pp -scattering including electromagnetic effects. Note that we have fixed the normalization of the correction factor $F_p(W)$ such that in the limit of vanishing scattering length a_p (i.e. vanishing final-state interaction), $F_p(W)$ becomes identical to one (in the effective range approximation).

With the help of Eqs.(5,6) we are now in the position to extract the values of $|\mathcal{A}|$ as shown in table 1. We ignore the point at the lowest energy since that close to threshold a better treatment of the infinite range Coulomb interaction in terms of proton wave functions would be needed. The empirical value of \mathcal{A} is thus

$$\mathcal{A}^{(\text{exp})} = (2.7 - i 0.3) \text{ fm}^4 , \quad (7)$$

anticipating the positive sign of the real part from the calculation in section 3. Since we are mostly interested in achieving a qualitative picture of the underlying production process, we refrain from assigning an uncertainty to this number. This number should be comparable to the one found by Adam et al. [23], who employ essentially the same method to correct for the final-state interaction but use a different (unspecified) normalization of the T-matrix. In Fig.2 we show the resulting total cross sections in comparison to the data of refs.[1, 2] using Eqs.(5,6,7).

T_{lab} [MeV]	282.2	285	290	295	300.3	308	314	319	325.6
σ_{tot} [μb]	0.148	0.56	1.31	2.06	3.07	4.47	5.25	6.18	7.71
$ \mathcal{A} $ [fm 4]	2.42	2.73	2.69	2.64	2.70	2.71	2.64	2.66	2.73

Table 1: Extracted values for the threshold amplitude $|\mathcal{A}|$ for the proton laboratory kinetic energies and cross sections of ref.[1].

3 Meson–exchange contributions

In this section, we work out a variety of one–boson exchange contributions related to chiral (pion) and non–chiral (vector meson) physics to the amplitude \mathcal{A} .

3.1 Tree level Goldstone boson contributions

In this and the following paragraph, we consider tree level and one–loop pion exchanges contributing to the $pp\pi^0$ production process at threshold. Due to the large proton momentum even at threshold, $|\vec{p}| \simeq \sqrt{mM_\pi}$, it is not appropriate to employ the frequently used heavy baryon formalism for the nucleons. Let us demonstrate the failure of the heavy baryon approach for a simple (but generic) example. Consider diagram b) in Fig.3 which involves a propagating nucleon after emission of the real π^0 . We show that this nucleon propagator can not be expanded in powers of $1/m$ in the usual way. Let $v^\mu = (1, \vec{0})$ be the four–vector which selects the center–of–mass frame. The four–vector of the propagating nucleon is $m v + k$ with $k^\mu = (-M_\pi/2, \vec{p})$ and $k^2 = -mM_\pi$. We start on the left hand side with the correct relativistic result and then perform the usual $1/m$ expansion of the heavy baryon formalism,

$$-\frac{1}{M_\pi} = \frac{2m}{(m v + k)^2 - m^2} = \frac{1}{v \cdot k + k^2/2m} = \frac{1}{v \cdot k} \sum_{n=0}^{\infty} \left(\frac{-k^2}{2m v \cdot k} \right)^n = -\frac{2}{M_\pi} \sum_{n=0}^{\infty} (-1)^n. \quad (8)$$

One sees that infinitely many terms of the $1/m$ –expansion contribute to the same order. The resulting series does not even converge and oscillates between zero and twice the correct answer. The source of this problem is the extreme kinematics of the reaction $NN \rightarrow NN\pi$ with $|\vec{p}| \simeq \sqrt{mM_\pi}$. In that case the leading order operator $\mathcal{O}^{(1)} = i v \cdot \partial$ and the next–to–leading order operator $\mathcal{O}^{(2)} = -\partial \cdot \partial/2m$ lead to the same result, here, $\pm M_\pi/2$. The heavy baryon formalism (and therefore also HBChPT) can not cope with external momenta as large as $|\vec{p}| \simeq \sqrt{mM_\pi}$. This problem is merely related to “trivial” kinematics and can be immediately overcome in fully relativistic calculations.^{#1} In the latter one does not presume that vertices and propagators can be consistently expanded in inverse powers of the large nucleon mass m . The occurrence of such non–expandable nucleon propagators is generic to $NN \rightarrow NN\pi$ and they will of course also enter in loop diagrams. In order to treat correctly the kinematics, one has to evaluate the loops relativistically, even though this may spoil the

^{#1}We can not entirely exclude the possibility of an alternative counting scheme in a suitably modified heavy fermion approach which could also do the job. We have, however, not been able to set up such a scheme.

one-to-one correspondence between the loop and small momentum/quark-mass expansion. A consistent power counting scheme for processes $NN \rightarrow NN\pi$ involving loops of arbitrary high order is not in sight at the moment.

We thus turn to the relativistic description of the chiral pion-nucleon system. Instead of giving the Lagrangian (see e.g. ref.[24]), we mention only the relevant pion-nucleon vertices. The πNN -vertex (and also the ηNN -vertex) is of pseudovector type as required by chiral symmetry. The second order isoscalar chiral $\pi\pi NN$ contact interaction, $\pi^0(q_1) + N(p_1) \rightarrow \pi^0(q_2) + N(p_2)$ reads,

$$\frac{i}{F_\pi^2} \left\{ -4c_1 M_\pi^2 + 2c_3 q_1 \cdot q_2 + \frac{c'_2}{2m} [(p_1 + p_2) \cdot q_1 \ q_2 + (p_1 + p_2) \cdot q_2 \ q_1] + \frac{c''_2}{2m^2} (p_1 + p_2) \cdot q_1 (p_1 + p_2) \cdot q_2 \right\}. \quad (9)$$

This form is unique since on mass-shell it gives the most general second order ($s \leftrightarrow u$) crossing symmetric polynomial contribution to the invariant isoscalar πN amplitudes,

$$A^+(s, u) = \frac{1}{F_\pi^2} \left\{ -4c_1 M_\pi^2 + c_3(s + u - 2m^2) + \frac{c''_2}{8m^2} (s - u)^2 \right\}, \quad B^+(s, u) = \frac{c'_2}{2mF_\pi^2} (s - u), \quad (10)$$

with s and u the usual Mandelstam variables. The low-energy constants c_1, c'_2, c''_2, c_3 have already been determined (at tree level) in [18] from low-energy πN data and we list their values for completeness:

$$c_1 = -0.64, \quad c'_2 = -5.63, \quad c''_2 = 7.41, \quad c_3 = -3.90, \quad (11)$$

all given in GeV^{-1} . As it was shown in ref. [25], the numerical values of most of these low-energy constants (c'_2, c''_2, c_3) can be understood largely from intermediate Δ excitations.

Consider first one-pion (π^0) exchange. The respective diagrams are shown in Figs. 3a,b (with $M = \pi^0$). We stress that these are relativistic Feynman graphs, i.e. in the intermediate states they contain the full relativistic fermion propagator which sums up several time-orderings. We also note that the graphs with the pion exchange after the emission of the π^0 from one of the proton lines does not belong to the final state-interaction according to our treatment (as an on-shell NN-process). We find

$$\mathcal{A}^{(\pi, \text{dir})} = \frac{g_{\pi N}^3}{4m^4(1 + \mu)(2 + \mu)} = 0.48 \text{ fm}^4, \quad (12)$$

with $g_{\pi N} = 13.4$ the strong pion-nucleon coupling constant. We remark that it is often claimed that the $pp\pi^0$ final-state should be suppressed due to chiral symmetry. This argument is based on the assumption of the exchanged pion being soft, which, however, is not the case. The $\pi^0 p$ amplitude with one π^0 off its mass-shell is only of linear order in the pion mass M_π (since $k^2 = -mM_\pi$) and this factor of M_π is cancelled by the pion propagator $[M_\pi(m + M_\pi)]^{-1}$. Consequently, as Eq.(12) shows, the amplitude in impulse approximation does not vanish in the chiral limit as it is often claimed. In fact, chiral symmetry does not distinguish the $pp \rightarrow pp\pi^0$ process from the other $NN \rightarrow NN\pi$ channels. Next, there is the so-called π^0 rescattering, as shown in Fig. 3c,

$$\mathcal{A}^{(\pi, \text{res})} = \frac{g_{\pi N} \mu}{F_\pi^2 m (1 + \mu)} \left[\frac{c_3}{2} + \left(1 + \frac{\mu}{4}\right) c'_2 + \left(1 + \frac{\mu}{4}\right)^2 c''_2 - 2c_1 \right] = 0.46 \text{ fm}^4, \quad (13)$$

with $F_\pi = 92.4$ MeV the pion decay constant. Again, there is a marked difference to the heavy baryon case. To leading order, the relativistic couplings c'_2 , c''_2 combine to give the $c_2 = c'_2 + c''_2$ term in the heavy baryon approach. In previous HBChPT calculations the c_2 term was found with an incorrect prefactor $1/2$. The relative factor of two in the relativistic calculation comes from the fact that products of nucleon and pion four-momenta are not dominated anymore by the term nucleon mass times pion energy. For the reaction $NN \rightarrow NN\pi$ the product of the nucleon and pion three-momenta can be equally large, since $|\vec{p}| \simeq \sqrt{mM_\pi}$.

Interestingly, the combination of low-energy constants in Eq.(13) is dominated (to about 90%) by the last term $\sim -2c_1$, which is related to the so-called pion-nucleon sigma-term, $\sigma_{\pi N}(0) = -4c_1 M_\pi^2$ (to leading order). Therefore the strength of the π^0 -rescattering (at threshold) is almost entirely due to this particular chiral symmetry breaking term. The effects from the $\Delta(1232)$ -resonance encoded in the low-energy constants c'_2 , c''_2 , c_3 turn out to be very small. In order to check this interpretation, we have evaluated the contributions from explicit $\Delta(1232)$ -excitations, using the Rarita-Schwinger formalism and the well-satisfied coupling constant relation $g_{\pi N \Delta} = 3g_{\pi N}/\sqrt{2}$. We find:

$$\mathcal{A}^{(\Delta)} = \frac{g_{\pi N}^3 \mu}{16m_\Delta^2 m^3 (1+\mu)} \left\{ \frac{m^2(4+\mu)(m_\Delta + m(1-\mu))}{m_\Delta^2 + m^2(2\mu-1)} \right. \\ \left. + (2Z-1)[4(1+Z)m_\Delta - m(2Z(3+\mu) + 1+\mu)] \right\} = 0.04 \text{ fm}^4 . \quad (14)$$

where we used for the off-shell parameter $Z = -0.3$, the value which maximizes the $\Delta(1232)$ -contribution to the P_{33} πN scattering volume. Such a value of Z is also consistent with neutral pion photoproduction off protons. The small value of $\mathcal{A}^{(\Delta)}$ confirms the interpretation of the rescattering contribution Eq.(13) given above.

The next Goldstone boson which can contribute is the $\eta(547)$. Consider the graphs in Figs. 3a,b with $M = \eta$. We find

$$\mathcal{A}^{(\eta)} = \frac{g_{\pi N} g_{\eta N}^2 \mu}{4m^2(M_\eta^2 + m^2\mu)(2+\mu)} = 0.02 \text{ fm}^4 , \quad (15)$$

where we have employed the SU(3) value for the ηN coupling constant together with the simplified ratio of the octet axial vector coupling constants $D/F = 1.5$, which leads to $g_{\eta N} = 4.6$. Since this contribution is tiny, the precise value of this coupling does not matter.

3.2 Pion loop effects

We do not attempt a full one-loop calculation here, but rather consider certain (simple) classes of loop graphs which are genuine to the process under consideration. We use minimal subtraction to eliminate divergences and set the renormalization scale equal to the proton mass m . For estimating the genuine size of pion loop effect, such a procedure ignoring renormalization via counterterms should be sufficient and the resulting numbers should be considered indicative.

Consider first a certain class of pion loop diagrams which involve the $\pi\pi$ interaction, compare Fig. 4. Notice that only the full class of diagrams is independent of the choice of

the interpolating pion field. Within the calculational scheme mentioned above, this class of graphs gives

$$\begin{aligned} \mathcal{A}^{(\text{loop},1)} &= \frac{g_{\pi N}^3 (2 + \mu)(1 - \mu)}{(8\pi m F_\pi)^2 (1 + \mu)} \left\{ \ln \mu - \frac{1}{2} + \sqrt{1 + 4\mu} \ln \frac{1 + \sqrt{1 + 4\mu}}{2\sqrt{\mu}} \right. \\ &\quad \left. + \int_0^1 dx \int_0^x dy \frac{y}{y^2 + \mu^2(1 - y) + \mu(1 - x)(x - y)} \right\} = -0.10 \text{ fm}^4 . \end{aligned} \quad (16)$$

We remark that the expression in the curly brackets is not singular in the chiral limit $\mu \rightarrow 0$. It has the following μ -expansion: $-1/2 + \sqrt{\mu} \pi^2/8 + \mathcal{O}(\mu \ln \mu)$. Again, one faces here the usual problem of relativistic loops. $\mathcal{A}^{(\text{loop},1)}$ does not vanish in the chiral limit $\mu \rightarrow 0$ and is therefore not suppressed by powers of the pion mass M_π compared to tree graphs. Nevertheless, its numerical value is small. The threshold amplitude $\mathcal{A}^{(\text{loop},1)}$ is actually proportional to the relativistic loop contribution [24] to the nucleon scalar form factor evaluated at an invariant momentum transfer squared $t = -m^2\mu$,

$$\mathcal{A}^{(\text{loop},1)} = \frac{g_{\pi N} (2 + \mu)(\mu - 1)}{12m F_\pi^2 M_\pi^2 (1 + \mu)} \sigma_{\pi N}(-m^2\mu)_{\text{loop}} . \quad (17)$$

Whereas ref.[16] claimed that these loop graphs were sizeable and are essential for a quantitative description of the data, we find that they give only a small -4% correction to the empirical value of \mathcal{A} . The reason for this discrepancy is to be found in the inappropriate application of the heavy baryon formalism to $pp \rightarrow pp\pi^0$ in ref.[16]. Next, we consider the entire class of loop graphs proportional to $g_{\pi N}/F_\pi^4$, see graphs in Fig.5 and Fig.6. Figs.5 (a) and (b) represent $\pi^+\pi^-$ exchange between protons (in form of a bubble diagram) before or after the emission of the neutral pion. We find:

$$\begin{aligned} \mathcal{A}^{(\text{loop},2)} &= \frac{g_{\pi N} (2 - \mu)\mu}{768\pi^2 F_\pi^4 (2 + \mu)} \left\{ (1 + 6\mu) \ln \mu - \frac{5}{6} - 4\mu + (1 + 4\mu)^{3/2} \ln \frac{1 + \sqrt{1 + 4\mu}}{2\sqrt{\mu}} \right\} \\ &= -0.01 \text{ fm}^4 . \end{aligned} \quad (18)$$

Note that these loop corrections vanish in the chiral limit $\mu \rightarrow 0$. In the class of diagrams proportional to $g_{\pi N}/F_\pi^4$ there is also π^0 -exchange between the protons with π^+ rescattering on one of the nucleons, see (c) and (d) in Fig.5. These graphs give

$$\begin{aligned} \mathcal{A}^{(\text{loop},3)} &= \frac{g_{\pi N} \mu}{[8\pi F_\pi^2 (1 + \mu)(1 - 2\mu)]^2} \left\{ (1 + \mu)(1 - 2\mu)(4 - 6\mu - \mu^2) + (11 - 16\mu + \mu^2 + \mu^3) \right. \\ &\quad \left. \cdot \mu^2 \ln \mu + \mu(1 + \mu)(2 - 2\mu - \mu^2) \sqrt{\mu(4 + \mu)} \ln \frac{2 + \mu + \sqrt{\mu(4 + \mu)}}{2} \right\} \\ &= 0.22 \text{ fm}^4 . \end{aligned} \quad (19)$$

This contribution vanishes again in the chiral limit $\mu \rightarrow 0$. Finally, there are graphs where a $\pi^+\pi^-$ -pair is emitted from one proton and the π^0 emission proceeds via charge exchange

from the other nucleon line, see Fig.6. Straightforward evaluation of these diagrams gives

$$\begin{aligned}
\mathcal{A}^{(\text{loop},4)} &= \frac{g_{\pi N} \mu}{(8\pi F_\pi^2)^2} \left\{ \frac{\mu(9\mu - 2 - \mu^2)}{2(1 + \mu)(1 - 2\mu)} + \frac{6 - 12\mu + 19\mu^2 + 2\mu^3 + \mu^4}{2(1 + \mu)^2(1 - 2\mu)^2} \mu^2 \ln \mu \right. \\
&\quad + \frac{\mu^2(2 - \mu)}{2(1 - 2\mu)^2} \sqrt{\mu(4 + \mu)} \ln \frac{2 + \mu + \sqrt{\mu(4 + \mu)}}{2} + \int_0^1 dx \int_0^x dy y \times \\
&\quad \left[\frac{2x - 2 - 5y + \mu(3 - 3x - y) + \mu^2(3 - x)}{y^2 + \mu(1 - x)(x - 3y) + \mu^2(1 - 2y + xy)} + \frac{2 - 2x - 3y + \mu(x - 1) + \mu^2}{y^2 + \mu(1 - x)(x + y) + \mu^2(1 - y)} \right] \} \\
&= -0.25 \text{ fm}^4 , \tag{20}
\end{aligned}$$

a contribution which again vanishes in the chiral limit. Summing all these various loop contributions in Eqs.(16,18,19,20), we find

$$\mathcal{A}^{(\text{loop})} = -0.14 \text{ fm}^4 , \tag{21}$$

which is a rather small number as compared to the tree level pion exchange or the vector meson contributions (section 3.3). We observe sizeable cancellations between the various classes of loop graphs and conclude therefore that these do not play a significant role for explaining the threshold amplitude \mathcal{A} . The imaginary part of \mathcal{A} is discussed in the appendix.

3.3 Heavy meson exchanges

Due to the large momenta involved, one expects additional contributions due to the exchange of heavier mesons, which are of much shorter range than the pion exchange considered so far. From the symmetry point of view such terms are much less constrained and thus exhibit a certain unavoidable model-dependence. Nevertheless, these terms can play a significant role as first stressed by Lee and Riska [7] and confirmed by Horowitz et al. [8]. We do not discuss here additional effects from vector meson nucleon form factors, which are a model-dependent (and unobservable) concept to account for the finite size of the hadrons involved. Note also that in a strict field-theoretical sense such form factors can not be uniquely defined. At the invariant momentum transfer $t = -0.127 \text{ GeV}^2$ the form factor effect is not expected to be large. For example, one expects a 10% effect for typical monopole form factors with cut-offs $\Lambda_{\omega,\rho} \simeq 1.5 \text{ GeV}$.

Consider first neutral vector mesons. We start with the $\omega(782)$. There is sizeable uncertainty about its coupling constant to the nucleon, extreme values are e.g. found in the dispersion-theoretical analysis of the nucleons electromagnetic form factors, $g_{\omega N} \simeq 21$ [27]. However, it is not clear how one has to transcribe such a value to the one-boson exchange picture of the NN force. In conventional boson-exchange models, the inclusion of the correlated $\pi\rho$ continuum allows one to work with a coupling constant that is compatible with the SU(3) value, $g_{\omega N} \simeq 9$ or the value $g_{\omega N} = 10.1 \pm 0.9$ found from forward NN-dispersion relations [28]. For a detailed discussion, see e.g. ref. [29]. There is agreement that the tensor-to-vector coupling ratio of the ω -meson is very small. If we set $\kappa_\omega = 0$ and use the coupling constant $g_{\omega N} = 10$, we get

$$\mathcal{A}^{(\omega)} = \frac{g_{\pi N} g_{\omega N}^2 (2 - \mu)}{2m^2(M_\omega^2 + m^2\mu)(2 + \mu)} = 1.35 \text{ fm}^4 , \tag{22}$$

which is quite sizeable. In a similar fashion, we evaluate the $\rho(770)$ contribution. Here, there is less debate about the coupling constant $g_{\rho N}$ and also, it is well established that the tensor-to-vector coupling ratio κ_ρ is large. For simplicity, we use $g_{\rho N} = 3$ (obtained from ρ -universality, $g_{\rho N} = g_\rho/2$ with $g_\rho = 6$) and $\kappa_\rho = 6$. That leads to

$$\mathcal{A}^{(\rho)} = \frac{g_{\pi N} g_{\rho N}^2}{2m^2(M_\rho^2 + m^2\mu)(2 + \mu)} \left[2 + \mu(\kappa_\rho^2 - \kappa_\rho - 1) + \mu^2 \kappa_\rho \left(1 + \frac{9}{8} \kappa_\rho \right) \right] = 0.48 \text{ fm}^4. \quad (23)$$

We note that this form is very different from what has been used in the literature so far, where one finds the ω, ρ -exchange to be proportional to $\mu(1 + \kappa_{\omega, \rho})$. We do not employ any inappropriate non-relativistic approximation here and thus obtain the results shown in Eqs.(22,23). Note that due to the large tensor-to-vector coupling ratio of the ρ -meson $\kappa_\rho = 6$ the terms proportional to μ and μ^2 in the square bracket of Eq.(23) are most important. We have also investigated the role of $\phi(1020)$ exchange, which can be related to the strangeness content of the nucleon wave function. The values of the ϕN coupling constant span a large range, as documented in table 2 of ref.[30]. To get a more precise number, we proceed as follows. We assume that the tensor-to-vector coupling ratios are given by the dispersive analysis of the nucleon electromagnetic form factors, $\kappa_\rho = 6.1$, $\kappa_\omega = -0.16$ and $\kappa_\phi = -0.22$ [27]. Using furthermore the SU(3) relation $g_{\omega N} = 3g_{\rho N} - \sqrt{2}g_{\phi N}$ [29] together with $g_{\rho N} = 2.63$ [31] and $g_{\omega N} = 10.1$ [28], we have $g_{\phi N} = -1.56$. This leads to $\mathcal{A}^{(V)} = \mathcal{A}^{(\rho)} + \mathcal{A}^{(\omega)} + \mathcal{A}^{(\phi)} = (0.38 + 1.40 + 0.02) \text{ fm}^4 = 1.80 \text{ fm}^4$, which is practically identical to the result obtained above using the simplified coupling constants. Thus, the sum of the vector meson contributions is fairly stable against parameter variations and also the $\phi(1020)$ does not play any role. Finally, we remark that substituting $(g_{\rho N}, M_\rho, \kappa_\rho)$ by $(e, 0, \kappa_\rho)$ one can convince oneself that the one-photon exchange gives a tiny correction of $\mathcal{A}^{(\gamma)} = 0.0085 \text{ fm}^4$, as it is of course expected.

Another mechanism, first proposed in this context in [13], is the emission of the neutral pion from the anomalous $\omega\rho\pi$ -vertex, with the $\rho(770)$ coupling to one and the $\omega(782)$ to the other proton. This type of graph is similar to well-known meson-exchange currents in electromagnetic processes. The pertinent interaction vertex, with its strength given by the coupling constant $G_{\omega\rho\pi}$, can be determined from the anomalous Wess-Zumino-Witten term for vector mesons (we only show the part of relevance here),

$$\mathcal{L}_{\omega\rho\pi} = -\frac{G_{\omega\rho\pi}}{F_\pi} \epsilon^{\mu\nu\alpha\beta} (\partial_\mu \omega_\nu) \vec{\rho}_\alpha \cdot \partial_\beta \vec{\pi}, \quad (24)$$

with $\epsilon^{\mu\nu\alpha\beta}$ the totally antisymmetric tensor in four dimensions ($\epsilon^{0123} = -1$). Using again the universal ρ -coupling, $g_\rho = 6$, the gauged Wess-Zumino-Witten term for vector mesons leads to the coupling constant

$$G_{\omega\rho\pi} = \frac{3g_\rho^2}{8\pi^2} = 1.37. \quad (25)$$

Similar values for $G_{\omega\rho\pi}$ have been found in refs.[32, 33] from systematic studies of $\omega(782)$ - and $\phi(1020)$ -decays. The contribution of the anomalous $\omega\rho\pi$ -vertex to \mathcal{A} is given by

$$\mathcal{A}^{(\omega\rho\pi)} = \frac{g_{\omega N} g_{\rho N} (1 + \kappa_\rho) G_{\omega\rho\pi} m \mu^2}{2F_\pi (M_\omega^2 + m^2\mu) (M_\rho^2 + m^2\mu)} = 0.09 \text{ fm}^4, \quad (26)$$

which is at first glance quite small. However, due to the two derivatives appearing in Eq.(24), one expects this contribution to be of much larger importance in the P-wave amplitudes. An analogous short range mechanism is the π^0 emission from the $a_0\eta\pi$ -vertex, proposed in ref.[13]. We have evaluated the respective contribution to \mathcal{A} and found that it is negligibly small, $\mathcal{A}^{(a_0\eta\pi)} = 0.003 \text{ fm}^4$. Finally, we do not consider a scalar meson exchange here. First, there is no scalar meson resonance which couples strongly to the nucleon and secondly, the fictitious “ $\sigma(550)$ ” of one-boson exchange models just simulates the long and intermediate range part of uncorrelated 2π -exchange in the NN interaction. The latter comes along with pion loops and is to some extent contained in the loop graphs considered above.

3.4 Total threshold amplitude

We are now in the position to evaluate the full amplitude \mathcal{A} from the various contributions. Combining Eqs.(12,13,15,21,22,23,26), we get

$$\begin{aligned}\mathcal{A}^{(\text{thy})} &= \mathcal{A}^{(\pi, \text{dir})} + \mathcal{A}^{(\pi, \text{res})} + \mathcal{A}^{(\eta)} + \mathcal{A}^{(\text{loop})} + \mathcal{A}^{(\omega)} + \mathcal{A}^{(\rho)} + \mathcal{A}^{(\omega\rho\pi)} \\ &= (0.48 + 0.46 + 0.02 - 0.14 + 1.35 + 0.48 + 0.09) \text{ fm}^4 \\ &= 2.74 \text{ fm}^4,\end{aligned}\quad (27)$$

which compares well with the empirical value given in Eq.(7). The resulting total cross section is shown in Fig. 2 as the dash-dotted line. Of course, taken the uncertainty in certain coupling constants and our simplified treatment of the final-state interaction, the 1% agreement between our theoretical prediction for \mathcal{A} and its empirical value, Eq.(7), should not be taken too serious. We only want to make the point that these well-known boson-exchange diagrams, when evaluated fully relativistically, can explain the near threshold data for $pp \rightarrow pp\pi^0$. Note also that the contribution from explicit $\Delta(1232)$ -excitation, cf. Eq.(14), is contained in the π^0 rescattering term via the low-energy constants c'_2, c''_2, c_3 .

4 Charged pion production in pp -collisions

In this section we will discuss charged pion production using the same approach. The T-matrix for charged pion production in proton-proton collisions, $p_1(\vec{p}) + p_2(-\vec{p}) \rightarrow p + n + \pi^+$, at threshold in the center-of-mass frame reads,

$$T_{\text{th}}^{\text{cm}}(pp \rightarrow pn\pi^+) = A_1 i(\vec{\sigma}_1 - \vec{\sigma}_2) \cdot \vec{p} + A_2 (\vec{\sigma}_1 \times \vec{\sigma}_2) \cdot \vec{p}. \quad (28)$$

Since there are no identical nucleons in the final state, the Pauli exclusion principle does not constrain the two complex threshold amplitudes A_1 and A_2 accompanying the symmetric pseudoscalar operators $i(\vec{\sigma}_1 - \vec{\sigma}_2) \cdot \vec{p}$ and $(\vec{\sigma}_1 \times \vec{\sigma}_2) \cdot \vec{p}$ to be equal. In fact the pn -system at rest can be in a spin-singlet or in a spin-triplet state. The threshold amplitude for the singlet transition ${}^3P_0 \rightarrow {}^1S_0 s$ is

$$A_1 + A_2 = \sqrt{2} \mathcal{A}, \quad (29)$$

which by isospin symmetry is related to the threshold amplitude \mathcal{A} for the reaction $pp \rightarrow pp\pi^0$ introduced in Eq.(1). Similarly, the threshold amplitude for the triplet transition ${}^3P_1 \rightarrow {}^3S_1 s$ is

$$A_1 - A_2 = \sqrt{2} \mathcal{B}, \quad (30)$$

and it has a phase of -28.1° equal to the 3P_1 pp phase shift at $T_{\text{lab}}^{\text{th}} = 292.3$ MeV. Because of this larger phase fixed by unitarity the imaginary part $\text{Im } \mathcal{B}$ will contribute non-negligibly to the total cross sections near threshold.

4.1 Extraction of the threshold amplitudes

Employing the same method as in section 2.2 to correct for the strong pn S-wave final-state interaction, the unpolarized total cross section for $pp \rightarrow pn\pi^+$ reads,

$$\begin{aligned}\sigma_{\text{tot}}(T_{\text{lab}}) = & \left(\frac{m}{4\pi}\right)^3 \frac{2\sqrt{T_{\text{lab}}}}{(2m + T_{\text{lab}})^{3/2}} \\ & \times \int_{m+m_n}^{W_{\text{max}}} \frac{dW}{W} \sqrt{\lambda(W^2, m^2, m_n^2) \lambda(W^2, M_{\pi^+}^2, 4m^2 + 2mT_{\text{lab}})} \\ & \times \left\{ |\mathcal{A}|^2 F_s(W) + |\mathcal{B}|^2 F_t(W) \right\}.\end{aligned}\quad (31)$$

The correction factors from the pn singlet and triplet S-wave final state interaction are given in the effective range approximation by

$$F_{s,t}(W) = \left\{ 1 + a_{s,t}(a_{s,t} + r_{s,t})P_*^2 + \frac{1}{4}a_{s,t}^2 r_{s,t}^2 P_*^4 \right\}^{-1}, \quad (32)$$

with W the final-state proton-neutron invariant mass and $W_{\text{max}} = \sqrt{4m^2 + 2mT_{\text{lab}}} - M_{\pi^+}$. m still denotes the proton mass and $m_n = 939.57$ MeV stands for the neutron mass. The quantity $P_*^2 = \lambda(W^2, m^2, m_n^2)/4W^2$ is the squared pn center-of-mass momentum. The singlet and triplet scattering lengths and effective range parameters for elastic np -scattering are taken from [22], their empirical values being $a_s = (23.748 \pm 0.010)$ fm, $a_t = (-5.424 \pm 0.004)$ fm, $r_s = (2.75 \pm 0.05)$ fm and $r_t = (1.759 \pm 0.005)$ fm. We neglect here the coupling between the 3S_1 and the 3D_1 pn -states, which should be very small at the energies under consideration. Such effects go beyond the accuracy of the effective range approximation and our treatment of the pn final-state interaction.

The data base of total cross sections for the process $pp \rightarrow pn\pi^+$ in the 30 MeV region above threshold consists at present of five data points measured at IUCF [4]. We leave out the data point at the highest energy $T_{\text{lab}} = 319.2$ MeV where the π^+ angular distributions are no more isotropic and thus P-waves start to become important. We also found it important to ignore the data point at the lowest energy $T_{\text{lab}} = 294.3$ MeV. Using Eq.(31) for the total cross section and the value of $|\mathcal{A}| = 2.72$ fm 4 as determined from the $pp \rightarrow pp\pi^0$ data, one finds in a least square fit of the remaining three data points for the modulus of the triplet threshold amplitude,

$$|\mathcal{B}| = 4.46 \text{ fm}^4, \quad (33)$$

with a very small total $\chi^2 = 0.044$. For these values of $|\mathcal{A}|$ and $|\mathcal{B}|$ the data point at $T_{\text{lab}} = 319.2$ MeV is underestimated by 17% in the S-wave approximation. An unconstrained fit of the same three data points gives $|\mathcal{A}| = 3.00$ fm 4 and $|\mathcal{B}| = 4.45$ fm 4 with a marginally smaller total $\chi^2 = 0.042$. It is quite remarkable that $|\mathcal{A}|$ is found to be in 10% agreement with the value obtained from fitting the many precise near threshold $pp \rightarrow pp\pi^0$ data. Due to the very strong pn final-state interaction in the 1S_0 exit channel ($a_s = 23.75$ fm) the singlet transition contributes a factor 30 to 40 less to the total cross section than the triplet transition. From our fit we get at the lowest energy $T_{\text{lab}} = 294.3$ MeV a total cross section of $0.57 \mu\text{b}$, compared to the experimental value of $(0.71 \pm 0.04) \mu\text{b}$ given in ref.[4]. Only if one widens the error band of this data point by the $\pm 15\%$ absolute normalization uncertainty it becomes (at the lower end) marginally consistent with the remaining data. If, however, the

data point at $T_{\text{lab}} = 294.3$ MeV were included in an unconstrained fit, very different values of the threshold amplitudes, $|\mathcal{A}| = 6.75$ fm 4 and $|\mathcal{B}| = 4.11$ fm 4 , would be found with a total $\chi^2 = 1.0$. In particular $|\mathcal{A}|$ would be a factor 2.5 larger than the one obtained from the fit to the $pp \rightarrow pp\pi^0$ data. Of course, such a large deviation from isospin symmetry is unacceptable.

Assuming a positive real part and using the information from the 3P_1 phase shift, one gets the following experimental value of the triplet threshold amplitude \mathcal{B} ,

$$\mathcal{B}^{(\text{exp})} = (3.9 - i 2.1) \text{ fm}^4 . \quad (34)$$

This number should be considered indicative since the systematic error of the extraction method is not under control when only three data points are fitted. Notice also that the imaginary part is fairly sizeable, quite different from \mathcal{A} , the threshold amplitude for $pp \rightarrow pp\pi^0$.

4.2 Diagrammatic approach

Next, we turn to the evaluation of the relativistic Feynman diagrams contributing to $pp \rightarrow pn\pi^+$ at threshold. In addition to the ones considered for $pp \rightarrow pp\pi^0$, there is now the possibility for isovector pion–rescattering. The chiral πN Lagrangian contains such vertices at leading order (the so-called Weinberg–Tomozawa vertex) and at next-to-leading order (a vertex proportional to the low-energy constant c_4). In fact there are always two isovector rescattering diagrams, one with a π^0 –exchange between the nucleons and another one with a π^+ being exchanged. The isospin factors are, however, such that both diagrams cancel identically (for any kinematics, not only at threshold). Of course, we neglect here the small isospin breaking due the different charged and neutral pion masses. For the other diagrams, one finds in most cases only an additional isospin factor of $\sqrt{2}$ compared to the case of $pp \rightarrow pp\pi^0$. To be specific, we get for pseudoscalar meson exchanges,

$$\mathcal{B}^{(j)} = \mathcal{A}^{(j)} , \quad (j = \pi \text{ dir}, \pi \text{ res}, \Delta, \eta) . \quad (35)$$

The vector meson contributions behave differently,

$$\mathcal{B}^{(\omega)} = \frac{g_{\pi N} g_{\omega N}^2}{2m^2(M_\omega^2 + m^2\mu)} = 1.56 \text{ fm}^4 , \quad (36)$$

$$\mathcal{B}^{(\rho)} = \frac{g_{\pi N} g_{\rho N}^2}{2m^2(M_\rho^2 + m^2\mu)(2 + \mu)} \left[2 + \mu(1 - \kappa_\rho - \kappa_\rho^2) - \mu^2 \kappa_\rho \left(1 + \frac{7}{8} \kappa_\rho \right) \right] \\ = -0.31 \text{ fm}^4 , \quad (37)$$

$$\mathcal{B}^{(\omega\rho\pi)} = -\mathcal{A}^{(\omega\rho\pi)} . \quad (38)$$

In the spirit of vector meson dominance one could also think of an isovector $\pi\rho NN$ contact vertex of the form $\bar{N} \gamma^\mu \gamma_5 \vec{\tau} \cdot (\vec{\rho}_\mu \times \vec{\pi}) N$ analogous to the Kroll–Ruderman term of charged pion photoproduction. However, the respective ρ^0 and ρ^+ exchange diagrams add up to zero by the same reason as given above for isovector pion–rescattering. We do not investigate in further detail pion loop effects for $pp \rightarrow pn\pi^+$, since they will turn out to be small in analogy to the case $pp \rightarrow pp\pi^0$ discussed in section 3.2 (for the classes of diagrams shown there). The

imaginary part of the amplitude \mathcal{B} can only be generated to one loop order by the two-pion exchange box diagrams evaluated in the appendix. It can, however, not be expected that the rather intricate energy dependence of the 3P_1 phase shift will be well described to one loop. This needs further study but goes beyond the scope of this paper. Summing up the various tree level contributions given in Eqs.(35,36,37,38) we get,

$$\mathcal{B}^{(\text{thy})} = 2.12 \text{ fm}^4 , \quad (39)$$

which in comparison to the experimental value in Eq.(34) is too small by a factor of about 2. Of course, one can not expect that the purely real tree diagrams evaluated here will reproduce accurately $\mathcal{B}^{(\text{exp})} = (3.9 - i 2.1) \text{ fm}^4$, whose imaginary part is about half as large as its real part. Certainly, there is important dynamics missing in our diagrammatic approach to the triplet amplitude \mathcal{B} . A more detailed discussion of the imaginary part of \mathcal{B} is given in the appendix.

We have done several checks on our treatment of the pn final-state interaction. First, we compared the effective range approximation with the empirical values of the 1S_0 and 3S_1 pn phase shifts in the energy range relevant here and found that deviations are smaller than 2%. Secondly, we have studied the π^+ production cross section as a function of the pn invariant mass W (given by Eq.(31) without dW -integration) and found good agreement with the data of [4], cf. Fig.7. From all this we conclude that our treatment of the pn final-state interaction is fairly realistic. Consequently, the underestimation in the π^+ production channel must be traced back to the on-shell triplet threshold amplitude \mathcal{B} .

A possible explanation is the initial-state interaction. The 3P_0 pp phase shifts are small and do not exceed values of -12° in the energy region $280 \text{ MeV} < T_{\text{lab}} < 325 \text{ MeV}$, relevant here. In contrast to this, the 3P_1 pp phase shifts are much larger with values around -30° . Therefore the initial-state interaction is relatively weak for the reaction $pp \rightarrow pp\pi^0$ near threshold which proceeds only via the 3P_0 entrance channel. On the other hand the cross sections for $pp \rightarrow pn\pi^+$ are mainly generated by the triplet transition ${}^3P_1 \rightarrow {}^3S_1s$ (the very strong 1S_0 pn final-state interaction suppresses the singlet transition ${}^3P_0 \rightarrow {}^1S_0s$) and in the 3P_1 entrance channel the initial-state interaction is much stronger. This may be the reason why our diagrammatic approach, which does not explicitly treat initial-state interactions, works very well in the case $pp \rightarrow pp\pi^0$ and less well in the case $pp \rightarrow pn\pi^+$.

Finally, we believe that all the features of the processes $pp \rightarrow pN\pi$ that we have learned here from the relativistic diagrammatic approach presented here will be useful for further studies within more complete dynamical models, which e.g. treat initial- and final-state interactions simultaneously. We also remark that a similar covariant one-boson exchange model has been developed in ref.[34], which describes the data at much higher energies, $0.3 \text{ GeV} < T_{\text{lab}} < 2.0 \text{ GeV}$. The same model has been applied to threshold data in ref.[35]. These others introduce in addition (unobservable) meson nucleon form factors and energy-dependent coupling constants. This makes a direct comparison between their work and ours very difficult. However, no isoscalar pion rescattering and no pion loops are considered. Similar to our finding it is concluded that $\omega(782)$ exchange is important close to pion production threshold and that the $\Delta(1232)$ plays no role.

5 Eta-meson production in pp -collisions

In this section we will discuss η -production using a similar approach. The T-matrix for η -production in proton-proton collisions, $p_1(\vec{p}) + p_2(-\vec{p}) \rightarrow p + p + \eta$, at threshold in the center-of-mass frame reads,

$$T_{\text{th}}^{\text{cm}}(pp \rightarrow pp\eta) = \mathcal{C} (i\vec{\sigma}_1 - i\vec{\sigma}_2 + \vec{\sigma}_1 \times \vec{\sigma}_2) \cdot \vec{p}. \quad (40)$$

with \mathcal{C} the (complex) threshold amplitude for η -production. The η -production threshold is reached at a proton laboratory kinetic energy $T_{\text{lab}}^{\text{th}} = M_\eta(2 + M_\eta/2m) = 1254.6$ MeV, where $M_\eta = 547.45$ MeV denotes the eta-meson mass.

5.1 Extraction of the threshold amplitude

In the case of η -production near threshold it is also important to take into account the ηp final-state interaction, since the ηN -system interacts rather strongly near threshold. In fact a recent coupled-channel analysis [36] of the $(\pi N, \eta N)$ -system finds for the real part of the ηN scattering length $\text{Re } a_{\eta N} = (0.717 \pm 0.030)$ fm. For comparison, this value is a factor 5.7 larger than the $\pi^- p$ scattering length, $a_{\pi^- p} = 0.125$ fm [37], measured in pionic hydrogen.

We assume that the correction due to the S-wave ηp final-state interaction near threshold can be treated in effective range approximation analogous to the S-wave pp final-state interaction. We furthermore make the assumption that the final state interactions in the pp subsystem and in the two ηp subsystems do not influence each other and that they factorize. These are of course very strong assumptions, but as we will see soon, such a simple ansatz for the final-state interaction in the $pp\eta$ three-body system allows to describe rather accurately the energy dependence of the total cross section $\sigma_{\text{tot}}(pp \rightarrow pp\eta)$ near threshold. Using the factorization ansatz mentioned before, the unpolarized total cross section for $pp \rightarrow pp\eta$ reads,

$$\begin{aligned} \sigma_{\text{tot}}(T_{\text{lab}}) &= |\mathcal{C}|^2 \left(\frac{m}{4\pi}\right)^3 \frac{2\sqrt{T_{\text{lab}}}}{(2m + T_{\text{lab}})^{3/2}} \int_{2m}^{W_{\text{max}}} dW W F_p(W) \\ &\times \int_{s_\eta^-}^{s_\eta^+} ds_\eta F_\eta(s_\eta) F_\eta(6m^2 + 2mT_{\text{lab}} + M_\eta^2 - W^2 - s_\eta). \end{aligned} \quad (41)$$

with $W_{\text{max}} = \sqrt{4m^2 + 2mT_{\text{lab}}} - M_\eta$ the endpoint of the di-proton invariant mass spectrum and $F_p(W)$ given by Eq.(6). The variable s_η is the invariant mass squared of the first ηp -pair and the argument of the last function $F_\eta(\tilde{s}_\eta)$ in Eq.(41), $\tilde{s}_\eta = 6m^2 + 2mT_{\text{lab}} + M_\eta^2 - W^2 - s_\eta$, is the invariant mass squared of the second ηp -pair. The expressions

$$s_\eta^\pm = 3m^2 + mT_{\text{lab}} + \frac{1}{2}(M_\eta^2 - W^2) \pm \frac{1}{2W} \sqrt{(W^2 - 4m^2)\lambda(W^2, M_\eta^2, 4m^2 + 2mT_{\text{lab}})} \quad (42)$$

give the boundaries of the $pp\eta$ three-body phase space in the (s_η, W^2) -plane. Obviously, the formula for the total cross section, Eq.(41), is invariant under the permutation of the two ηp -pairs, $s_\eta \leftrightarrow \tilde{s}_\eta$, since $s_\eta^\pm = \tilde{s}_\eta^\mp$. Furthermore, the correction factor $F_\eta(s_\eta)$ due to the S-wave ηp final-state interaction reads in effective range approximation,

$$F_\eta(s_\eta) = \left| \frac{f_{\eta N}^{0+}(s_\eta)}{a_{\eta N}} \right|^2 = \left| 1 - \frac{i a_{\eta N}}{2\sqrt{s_\eta}} \sqrt{\lambda(s_\eta, M_\eta^2, m^2)} + \frac{a_{\eta N} r_{\eta N}}{8s_\eta} \lambda(s_\eta, M_\eta^2, m^2) \right|^{-2}. \quad (43)$$

Here, $f_{\eta N}^{0+}(s_\eta)$ is the S-wave ηN elastic scattering amplitude. The (complex) ηN scattering length $a_{\eta N} = ((0.717 \pm 0.030) + i(0.263 \pm 0.025))$ fm is taken from ref.[36] and the (complex) ηN effective range parameter $r_{\eta N} = ((-1.50 \pm 0.13) - i(0.24 \pm 0.04))$ fm stems from ref.[38]. It is important to note that both ref.[36] and ref.[38] using quite different methods agree within error bars on the value of the ηN scattering length $a_{\eta N}$.

Using Eq.(41,42,43) for the total cross section and the central values of $a_{\eta N}$ and $r_{\eta N}$ one finds in a least square fit of the six data points from CELSIUS [5] for the modulus of the threshold amplitude

$$|\mathcal{C}| = 1.32 \text{ fm}^4, \quad (44)$$

with a total $\chi^2 = 3.8$. The resulting energy dependent cross section from threshold up to $T_{\text{lab}} = 1375$ MeV is shown in Fig. 8 together with the data from CELSIUS [5].^{#2} It is rather astonishing that one can describe the total cross section data up to 100 MeV above threshold with a constant threshold amplitude \mathcal{C} and a simple factorization ansatz for the three-body final-state interaction.

5.2 Diagrammatic approach

Next, we turn to evaluation of the relativistic Feynman diagrams contributing to $pp \rightarrow pp\eta$ at threshold. The resulting expressions can essentially be copied from the case $pp \rightarrow pp\pi^0$ making only the substitution $(g_{\pi N}, M_\pi) \rightarrow (g_{\eta N}, M_\eta)$. One finds for $\pi^0, \eta, \omega, \rho^0$ -exchange

$$\mathcal{C}^{(\pi^0)} = \frac{g_{\eta N} g_{\pi N}^2 M_\eta}{4m^2 (M_\pi^2 + m M_\eta) (2m + M_\eta)} = 0.17 \text{ fm}^4, \quad (45)$$

$$\mathcal{C}^{(\eta, \text{dir})} = \frac{g_{\eta N}^3}{4m^2 (m + M_\eta) (2m + M_\eta)} = 0.02 \text{ fm}^4, \quad (46)$$

$$\mathcal{C}^{(\omega)} = \frac{g_{\eta N} g_{\omega N}^2 (2m - M_\eta)}{2m^2 (M_\omega^2 + m M_\eta) (2m + M_\eta)} = 0.23 \text{ fm}^4, \quad (47)$$

$$\begin{aligned} \mathcal{C}^{(\rho^0)} &= \frac{g_{\eta N} g_{\rho N}^2}{2m (M_\rho^2 + m M_\eta) (2m + M_\eta)} \\ &\times \left[2 + \frac{M_\eta}{m} (\kappa_\rho^2 - \kappa_\rho - 1) + \frac{M_\eta^2}{m^2} \kappa_\rho \left(1 + \frac{9}{8} \kappa_\rho \right) \right] = 0.50 \text{ fm}^4. \end{aligned} \quad (48)$$

Note that the ρ^0 exchange has become dominant because of the large tensor-to-vector coupling ratio $\kappa_\rho = 6$ and the larger ratio $M_\eta/m = 0.58$. Besides these diagrams with η -emission before and after meson exchange between the protons, one has to account for the strong ηp rescattering. Microscopically, the strong ηN S-wave interaction originates (among other things) from the nucleon resonance $S_{11}(1535)$ which is supposed to have a very large coupling to the ηN -channel. Instead of introducing this resonance together with several parameters (mass, width, coupling constant), we will merely introduce here a local $NN\eta\eta$ contact vertex of the form

$$\mathcal{L}_{\eta N} = K \bar{N}(x) N(x) \eta^2(x). \quad (49)$$

^{#2}Earlier data from SATURNE [39, 40, 41] do not have the same accuracy and are not considered further.

The interaction strength K is then determined by the real part of the ηN scattering length. This means that the pseudovector Born graphs plus the contact vertex sum up to give the empirical value of $\text{Re } a_{\eta N} = 0.717 \text{ fm}$. This leads to the equation

$$4\pi\left(1 + \frac{M_\eta}{m}\right) \text{Re } a_{\eta N} = 2K - \frac{g_{\eta N}^2 M_\eta^2}{m(4m^2 - M_\eta^2)} , \quad (50)$$

which results in a value of $K = 7.41 \text{ fm}$. The η –rescattering graph (analogous to Fig. 3c) leads to the following contribution to the threshold amplitude,

$$\mathcal{C}^{(\eta, \text{res})} = \frac{g_{\eta N} K}{m M_\eta (m + M_\eta)} = 0.40 \text{ fm}^4 . \quad (51)$$

Evidently, all contributions to \mathcal{C} scale with the (empirically not well determined) ηN –coupling constant $g_{\eta N}$. The numbers given in Eqs.(45,46,47,48,51) which add up to the empirical value of $|\mathcal{C}| = 1.32 \text{ fm}^4$ follow with $g_{\eta N} = 5.3$. Such a value of $g_{\eta N}$ is consistent with all existing empirical information on it. The SU(3) flavor symmetry connects the pion–nucleon and eta–nucleon coupling constants via the D/F ratio (of the baryon octet axial vector couplings),

$$g_{\eta N} = g_{\pi N} \frac{3 - D/F}{\sqrt{3}(1 + D/F)} . \quad (52)$$

Using $g_{\pi N} = 13.4$, the for our purpose optimal value $g_{\eta N} = 5.3$ requires a ratio $D/F = 1.37$. In fact a systematic analysis of semileptonic hyperon decays in ref.[42] gives $D/F = 1.58 \pm 0.07$, not far from this number. Of course, SU(3) is broken to some extent by the strange quark mass. For a recent update, see e.g. [43]. There is one further contribution we have not discussed so far, related to the $a_0 - \eta - \pi$ coupling. This coupling is rather uncertain. If one assumes that the diagrams with η –emission from the $a_0 \eta \pi$ –vertex contribute with a positive sign,

$$\mathcal{C}^{(a_0 \eta \pi)} = \frac{g_{a_0 N} g_{\pi N} (c_d M_\eta^2 - 2c_m M_\pi^2)}{\sqrt{6} m F_\pi^2 (M_{a_0}^2 + m M_\eta) (M_\pi^2 + m M_\eta)} = 0.05 \text{ fm}^4 , \quad (53)$$

one can even lower the ηN –coupling constant to $g_{\eta N} = 5.1$. We used here $g_{a_0 N} = 4.5$ [44] and $c_d = 32 \text{ MeV}$, $c_m = 42 \text{ MeV}$ [45]. We also note the one–boson exchange model of [44] for elastic NN scattering uses an ηN –coupling constant of $g_{\eta N}^{\text{OBE}} = 6.8$ not far from our value $g_{\eta N} = 5.3$.

The main point we want to make here is that even the $pp \rightarrow pp\eta$ threshold amplitude can be understood in terms of these well–known meson exchange diagrams when evaluated relativistically. With rather mild assumptions on the coupling constant $g_{\eta N}$ and the form of the ηN –rescattering one can easily reproduce the empirical value $|\mathcal{C}| = 1.32 \text{ fm}^4$. For another boson–exchange approach to η –production, see e.g. [46] (and references therein).

5.3 Comments on η' -production near threshold

Finally, we like to comment on the recent η' -production data near threshold from COSY [47] and SATURNE [41]. Taken face value, the energy dependence of the four COSY cross section data points is best described by the pure three-body phase space behavior (as shown by the dotted curve in Fig. 2 of ref.[47]). Of course, it is hard to imagine that the pp final-state interaction does not play a role for $pp \rightarrow pp\eta'$ that close to threshold where these data were measured. We have analyzed the combined COSY and SATURNE data (six data points) within our approach including the pp final-state interaction in effective range approximation. Only if one ignores the COSY data at the two lowest energies (at cm excess energies of 1.5 and 1.7 MeV, respectively), one can fit the remaining four data points with a modulus of the threshold amplitude of $|\mathcal{C}'| = 0.21 \text{ fm}^4$ with a small total $\chi^2 = 2.4$. This fit leads to values of the total cross section at the two lowest energy points of 5.2 nb and 6.3 nb (see also table 2). These numbers are more than twice as large as the corresponding central values given in ref.[47]. Presumably, the discrepancy results from the background subtraction which becomes most difficult very close to threshold. This deserves further study.

Q [MeV]	1.5	1.7	2.9	3.7	4.1	8.3
$\sigma_{\text{tot}}^{\text{exp}}$ [nb]	2.5 ± 0.5	2.9 ± 1.1	12.7 ± 3.2	19.2 ± 2.7	25.2 ± 3.6	43.6 ± 6.5
$\sigma_{\text{tot}}^{\text{fit}}$ [nb]	5.23	6.29	13.34	18.45	21.09	50.13

Table 2: Total cross section for $pp \rightarrow pp\eta'$ as a function of the cm excess energy $Q = \sqrt{4m^2 + 2mT_{\text{lab}}} - 2m - M_{\eta'}$ (only the mean value is given). The data are from refs.[41, 47]. The fit is described in the text.

Within the relativistic one-boson ($\pi^0, \eta, \omega, \rho^0$) exchange model the fit value $|\mathcal{C}'| = 0.21 \text{ fm}^4$ implies the relation $g_{\eta'N}(1 - 1.28\epsilon) = 1.12$. Here $g_{\eta'N}$ denotes the $\eta'N$ -coupling constant and ϵ is the fraction of pseudoscalar $\eta'NN$ -coupling (since the $\eta'(958)$ is no Goldstone boson there is no reason to favor the pseudovector coupling). Interestingly, only the tensor interaction of the ρ -exchange ($\sim \kappa_\rho$) is sensitive to the parameter ϵ .

According to ref.[48] one can relate the $\eta'N$ -coupling constant to the quark helicity contribution to the proton spin, $\Delta\Sigma = \sqrt{3/2}g_{\eta'N}F_\pi/m + 0.15$. Using the recent determination $\Delta\Sigma = 0.45 \pm 0.09$ of ref.[49] from polarized deep inelastic lepton scattering, one can extract within the relativistic one-boson exchange model an $\eta'N$ -coupling constant of $g_{\eta'N} = 2.5 \pm 0.7$ and a pseudoscalar coupling fraction of $\epsilon = 0.4 \pm 0.1$. It remains to be seen whether other η' -production processes (e.g. photoproduction $\gamma p \rightarrow \eta'p$) are consistent with these values.

A Imaginary parts from one-pion loop graphs

In this appendix we will give explicit expressions for the imaginary parts of the pion production threshold amplitudes $\text{Im } \mathcal{A}$ and $\text{Im } \mathcal{B}$ as they arise in one-pion loop approximation. To that order any non-vanishing imaginary part can only come from those one-loop diagrams which involve proton rescattering in the initial state. These are just the two-pion exchange box diagrams shown in Fig. 9. We apply the Cutkosky cutting rules to evaluate their imaginary part. It is then given by the product of the upper tree-level subgraph (i.e. the threshold pion production amplitude with 1π -exchange) and of one-half the invariant pp two-body phase space times the lower tree-level subgraph. The latter two factors combine to the 3P_0 or 3P_1 pp phase shift calculated perturbatively in 1π -exchange approximation at $T_{\text{lab}}^{\text{th}} = M_\pi(2 + M_\pi/2m)$. Altogether one gets thus from perturbative unitarity,

$$\text{Im } \mathcal{A} = \mathcal{A}^{(\pi, \text{dir})} \cdot \delta_{1\pi}({}^3P_0) , \quad (\text{A.1})$$

$$\text{Im } \mathcal{B} = \mathcal{B}^{(\pi, \text{dir})} \cdot \delta_{1\pi}({}^3P_1) , \quad (\text{A.2})$$

with $\mathcal{A}^{(\pi, \text{dir})}$ and $\mathcal{B}^{(\pi, \text{dir})}$ given in Eqs.(12,35). Using the projection formulas of ref.[50] to calculate the 1π -exchange ${}^3P_{0,1}$ phase shifts one finds the following analytical results,

$$\text{Im } \mathcal{A} = \frac{g_{\pi N}^5 \sqrt{\mu(4 + \mu)}}{64\pi m^4(1 + \mu)(2 + \mu)^2} \left[1 - \frac{\mu}{4 + \mu} \ln \left(2 + \frac{4}{\mu} \right) \right] = 0.54 \text{ fm}^4 , \quad (\text{A.3})$$

$$\text{Im } \mathcal{B} = \frac{g_{\pi N}^5 \sqrt{\mu(4 + \mu)}}{64\pi m^4(1 + \mu)(2 + \mu)^2} \left[\frac{\mu - 4}{2(4 + \mu)} - \frac{\mu^2}{(4 + \mu)^2} \ln \left(2 + \frac{4}{\mu} \right) \right] = -0.29 \text{ fm}^4 . \quad (\text{A.4})$$

One observes that in one-pion loop approximation $\text{Im } \mathcal{A}$ is too large by a factor of 2 with the wrong (positive) sign, whereas $\text{Im } \mathcal{B}$ is too small by a factor of 7. Clearly, there is important short range NN-dynamics missing in one-pion loop approximation as can be seen by comparing the empirical ${}^3P_{0,1}$ phase shifts at $T_{\text{lab}}^{\text{th}} = M_\pi(2 + M_\pi/2m)$, $\delta({}^3P_0) = -6.3^\circ$ and $\delta({}^3P_1) = -28.1^\circ$, with the 1π -exchange approximation, $\delta_{1\pi}({}^3P_0) = +65.0^\circ$ and $\delta_{1\pi}({}^3P_1) = -34.6^\circ$.

References

- [1] H.O. Meyer et al., Phys. Rev. Lett. 65 (1990) 2846; Nucl. Phys. A539 (1992) 663.
- [2] A. Bondar et al., Phys. Lett. B356 (1995) 8.
- [3] M. Drochner et al., Phys. Rev. Lett. 77 (1996) 454;
C. Heimberg et al., Phys. Rev. Lett. 77 (1996) 1012.
- [4] J.G. Hardie et al., Phys. Rev. C56 (1997) 20.
- [5] H. Calen et al., Phys. Lett. B366 (1996) 39.
- [6] G. Miller and P. Sauer, Phys. Rev. C44 (1991) 1725.
- [7] T.-S.H. Lee and D.O. Riska, Phys. Rev. Lett. 70 (1993) 2237.
- [8] C.J. Horowitz, H.O. Meyer and D.K. Griegel, Phys. Rev. C49 (1994) 1337.
- [9] E. Hernandez and E. Oset, Phys. Lett. B350 (1995) 158.

- [10] C. Hanhart, J. Haidenbauer, A. Reuber, C. Schütz and J. Speth, Phys. Lett. B358 (1995) 21.
- [11] B.Y. Park, F. Myhrer, J.R. Morones, T. Meissner and K. Kubodera, Phys. Rev. C53 (1996) 1519.
- [12] T.D. Cohen, J.L. Friar, G.A. Miller and U. van Kolck, Phys. Rev. C53 (1996) 2661.
- [13] U. van Kolck, G.A. Miller and D.O. Riska, Phys. Lett. B388 (1996) 679.
- [14] T. Sato, T.-S.H. Lee, F. Myhrer and K. Kubodera, Phys. Rev. C56 (1997) 1246.
- [15] C. Hanhart, J. Haidenbauer, M. Hoffmann, Ulf-G. Meißner and J. Speth, Phys. Lett. B424 (1998) 8.
- [16] E. Gedalin, A. Moalem and L. Razdolskaya, [nucl-th/9803029].
- [17] M.E. Schillaci, R.E. Silbar and J.E. Young, Phys. Rev. 179 (1969) 1539.
- [18] V. Bernard, N. Kaiser and Ulf-G. Meißner, Nucl. Phys. B475 (1995) 147.
- [19] V. Bernard, N. Kaiser, Ulf-G. Meißner and A. Schmidt, Nucl. Phys. A580 (1994) 475; V. Bernard, N. Kaiser and Ulf-G. Meißner, Phys. Lett. B382 (1996) 19.
- [20] V. Bernard, N. Kaiser and Ulf-G. Meißner, Nucl. Phys. A619 (1997) 261.
- [21] K.M. Watson, Phys. Rev. 88 (1952) 1163.
- [22] O. Dumbrajs et al., Nucl. Phys. B216 (1983) 277.
- [23] J. Adam, A. Stadler, M.T. Pena and F. Gross, Phys. Lett. B407 (1997) 97.
- [24] J. Gasser, M.E. Sainio and A. Švarc, Nucl. Phys. B307 (1988) 779.
- [25] V. Bernard, N. Kaiser and Ulf-G. Meißner, Nucl. Phys. A615 (1997) 483.
- [26] V. Bernard, N. Kaiser and Ulf-G. Meißner, Int.J. Mod. Phys. E4 (1995) 193.
- [27] P. Mergell, Ulf-G. Meißner and D. Drechsel, Nucl. Phys. A596 (1996) 367.
- [28] W. Grein and P. Kroll, Nucl. Phys. A338 (1980) 332; Nucl. Phys. A377 (1982) 505.
- [29] K. Holinde, Prog. Part. Nucl. Phys. 36 (1996) 311.
- [30] Ulf-G. Meißner, V. Mull, J. Speth and J.W. Van Orden, Phys. Lett. B408 (1997) 381.
- [31] G. Höhler and E. Pietarinen, Nucl. Phys. B95 (1975) 210.
- [32] P. Jain, R. Johnson, Ulf-G. Meißner, N.W. Park and J. Schechter, Phys. Rev. D37 (1988) 3252.
- [33] F. Klingl, N. Kaiser and W. Weise, Z. Phys. A356 (1996) 193.
- [34] A. Engel, R. Shyam, U. Mosel and A.K. Dutt–Mazumder, Nucl. Phys. A603 (1996) 387.
- [35] R. Shyam and U. Mosel, [nucl-th/9611013].
- [36] M. Batinic, I. Slaus, A. Švarc and B.M.K. Nefkens, Phys. Rev. C51 (1995); (E) Phys. Rev. C57 (1998) 1004; M. Batinic, I. Dadic, I. Slaus, A. Švarc, B.M.K. Nefkens and T.-S.H. Lee, Physica Scripta (1998) in print. The value for $a_{\eta N}$ is taken from the last reference.
- [37] D. Sigg et al., Nucl. Phys. A609 (1996) 269; (E) Nucl. Phys. A617 (1997) 526.
- [38] A.M. Green and S. Wycech, Phys. Rev. C55 (1997) R2167.
- [39] E. Chiavassa et al., Phys. Lett. B322 (1994) 270.
- [40] A.M. Bergdolt et al., Phys. Rev. D48 (1993) R2969.
- [41] F. Hibou et al., [nucl-ex/9802002] (to be published).
- [42] M. Bourquin et al., Z. Phys. C21 (1983) 27.
- [43] P.G. Ratcliffe. Phys. Lett. B365 (1996) 383.
- [44] R. Machleidt, K. Holinde and C. Elster, Phys. Rep. 149 (1987) 1.
- [45] G. Ecker, J. Gasser, A. Pich and E. de Rafael, Nucl. Phys. B321 (1989) 311.
- [46] A. Moalem et al., Nucl. Phys. A589 (1995) 649; Nucl. Phys. A600 (1996) 445.
- [47] P. Moskal et al., Phys. Rev. Lett. 80 (1998) 3202.
- [48] A.V. Efremov, J. Soffer and N.A. Törnqvist, Phys. Rev. D44 (1991) 1369.
- [49] G. Altarelli, R.D. Ball, S. Forte and G. Ridolfi, Nucl. Phys. B496 (1997) 337.
- [50] N. Kaiser, R. Brockmann and W. Weise, Nucl. Phys. A625 (1997) 758.

Figures

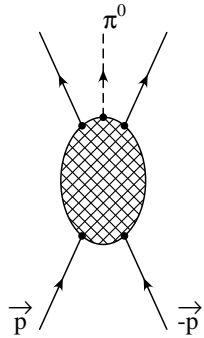


Figure 1: The process $pp \rightarrow pp\pi^0$ in the center-of-mass system.

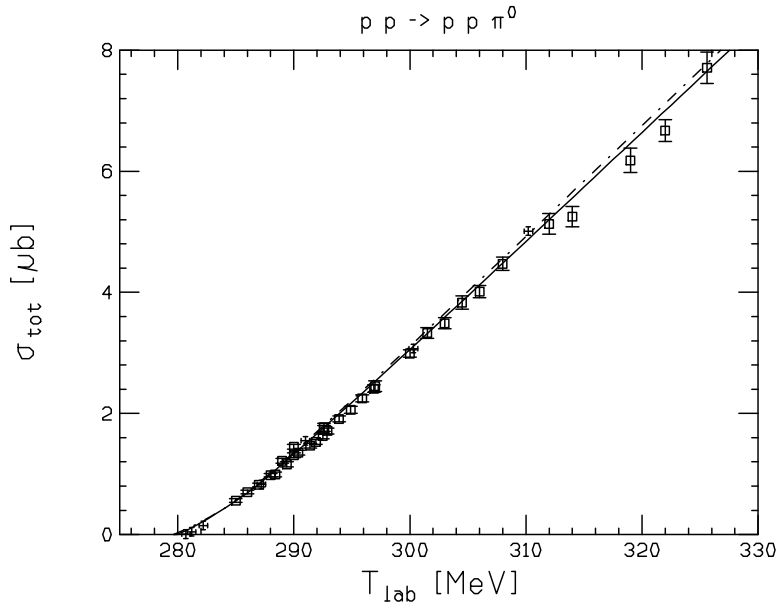


Figure 2: Fit to the total cross section for $pp \rightarrow pp\pi^0$ as described in the text (solid line). The data are from [1] (boxes) and [2] (crosses). The dashed line is explained in sec. 3.4.

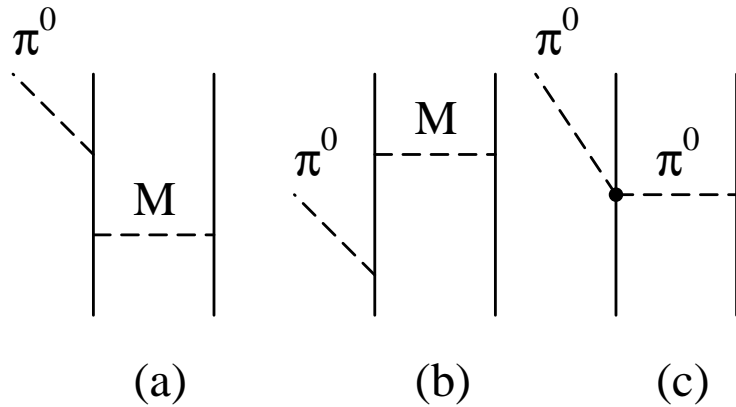


Figure 3: Feynman graphs for neutral pion production. (a) and (b) are the direct terms, with meson exchange $M = \pi^0, \eta, \omega, \rho^0$. (c) is the rescattering graph. The heavy dot denotes the second order isoscalar chiral $\pi\pi NN$ -vertex. Graphs where the pion (dashed line) is emitted from the other proton (solid) line and graphs with crossed outgoing proton lines are not shown.

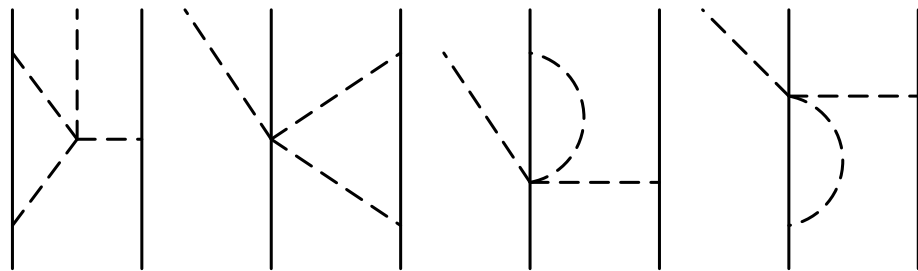


Figure 4: Class of one loop graphs involving the $\pi\pi$ interaction. For further notation, see Fig.3.

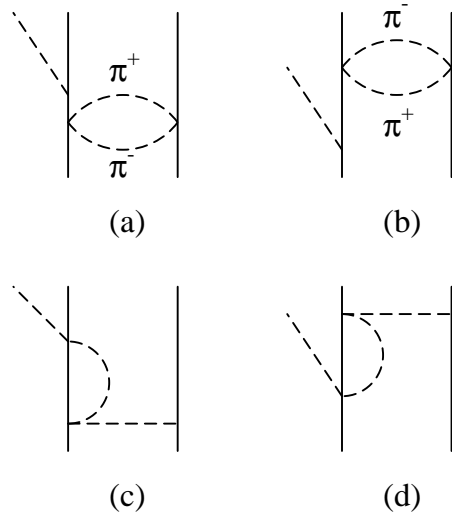


Figure 5: Further loop diagrams proportional to $g_{\pi N}/F_\pi^4$. (a) and (b) represent $\pi^+\pi^-$ exchange between protons, (c) and (d) are the π^+ rescattering diagrams. For further notation, see Fig.3.

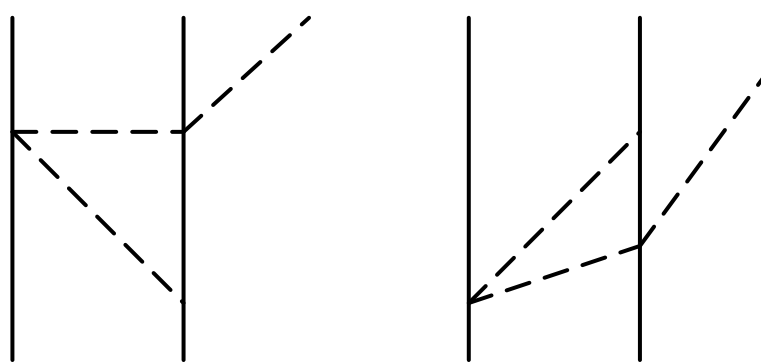


Figure 6: Loop diagrams with π^0 emission via charge exchange. For further notation, see Fig.3.

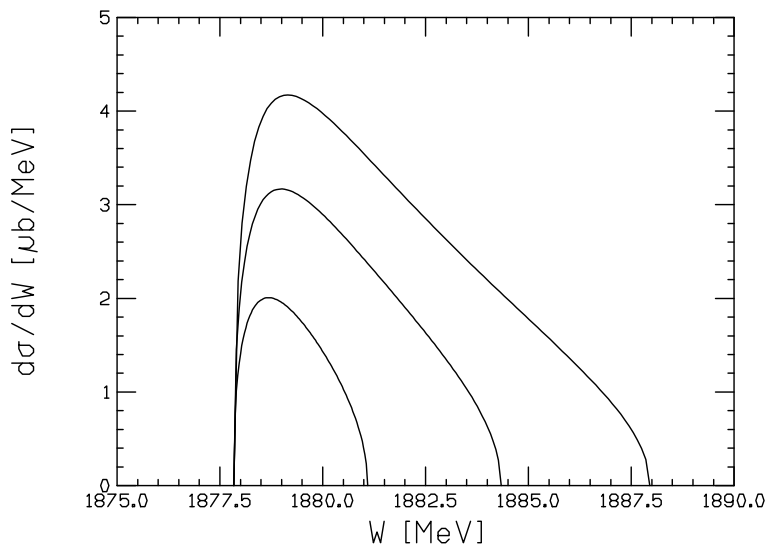


Figure 7: Pion production cross section as a function of the pn invariant mass W . The three curves corresponds to $T_{\text{lab}} = 299.3, 306.3$ and 314.1 MeV, in ascending order.

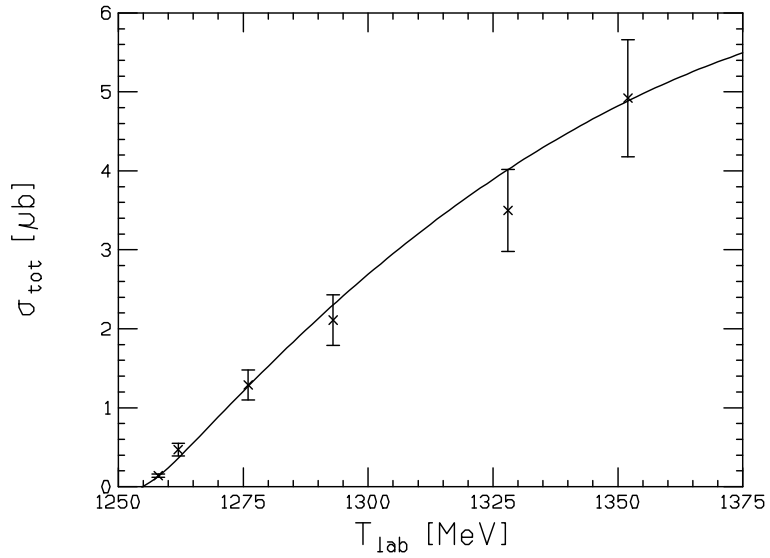


Figure 8: The eta-production cross section $\sigma_{\text{tot}}(pp \rightarrow pp\eta)$ as a function of T_{lab} . The data are taken from ref.[5].

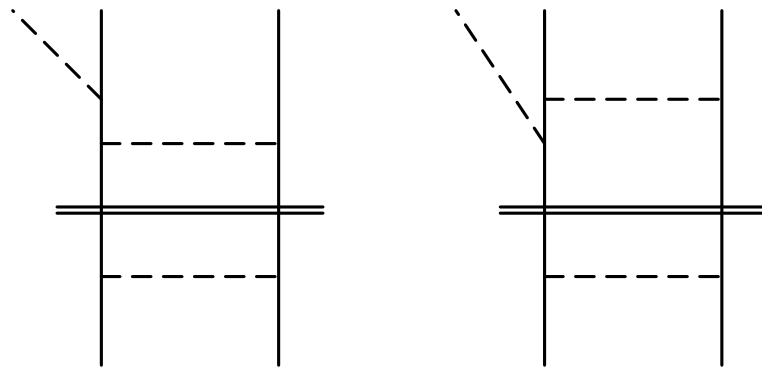


Figure 9: Diagrams that give rise to the non-vanishing imaginary parts $\text{Im } \mathcal{A}$ and $\text{Im } \mathcal{B}$ in one-pion loop approximation. The projection on the on-shell pp intermediate state is symbolized by the double line cutting the diagrams. For further notation, see Fig. 3.